Characterization of InP sensors for future thin-film detectors

Jennifer Ott[a], E.R. Almazan[a], S. Kim[b,c], T. Affolder[a], V. Fadeyev[a], J. Metcalfe[b], M. Hance[a], J. Nielsen[a]

a) Santa Cruz Institute for Particle Physics
b) Argonne National Laboratory
c) University of Illinois at Chicago

42nd RD50 Workshop, 20.-23. June 2023

*jeott@ucsc.edu

Motivation

- Finely segmented silicon tracking detectors are the core of particle physics experiments
- Drivers: fabrication of large areas – cost, power consumption, material budget, hybridization technology…
  - Excellent developments demonstrated in thin, large-area Si CMOS detectors, such as ALICE ITS3!
- Increasing demand also for good timing resolution and potentially energy resolution

➢ **Could other materials have an advantage over Si in some areas?**

- Ingot-based fabrication is expensive and time-consuming, not conveniently available for many materials

➢ **Thin film deposition methods provide access to a wider selection of insulators and semiconductors, by physical or chemical vapor deposition techniques from liquid or gas phase**

  ➢ Including epitaxial Si! ☺

- In the future: cost-effective deposition of thin layers, processing of integrated circuitry, on flexible substrates?

- Initial study – comparison of Si, InP, CdTe and diamond single pad sensors – conducted earlier by S. Kim and J. Metcalfe

J. Metcalfe et al, Potential of Thin Films for use in Charged Particle Tracking Detectors, arXiv:1411.1794

S. Kim et al, Thin film charged particle trackers, arXiv: 2209.08149

Other semiconductor materials

- This study: focus on Indium Phosphide

TABLE I

PROPERTIES OF SEMICONDUCTOR MATERIALS AT 25°C

Material	Atomic Number	Density g/cm³	Band-gap eV	Melting Point °C	Knoop Hardness	Crystal Structure	Ionicity	Dielectric Constant
Ge	32	5.33	0.67	958	692	Cubic	0	16
Si	14	2.33	1.12	1412	1150	Cubic	0	11.7
CdTe	48, 52	6.2	1.44	1092	45	Hexagonal	0.61	11
CdZnTe	48, 30, 52	≈ 6	1.5–2.2	1092–1295				
CdSe	48, 34	5.81	1.73	>1350		Hexagonal	0.6	10.6
CdZnSe	48, 30, 34	≈ 5.5	1.7–2.7	1239–1520				
HgI_2	80, 53	6.4	2.13	250 (127†)	<10	Tetragonal	0.67	8.8
TlBrI	81, 35, 53	7.5	2.2–2.8	405–480	40	Cubic		
GaAs	31, 33	5.32	1.43	1238	750	Cubic	0.23	12.8
InI	49, 53	5.31	2.01	351	27	Orthorhombic	0.8	26
GaSe	31, 34	4.55	2.03	960		Hexagonal	0.53	8
diamond	6	3.51	5.4	4027	10^4	Cubic	0	5.5
TlBr	81, 35	7.56	2.68	480	12	Cubic	0.81	29.8
PbI_2	82, 53	6.2	2.32	402	<10	Hexagonal	0.8	
InP	49, 15	4.78	1.35	1057	535	Cubic	0.38	12.5
ZnTe	30, 52	5.72	2.26	1295		Cubic	0.62	9.7
HgBrI	80, 35, 53	6.2	2.4–3.4	229–259	14	Orthorhombic		
a-Si	14	2.3	1.8				0	11.7
a-Se	34	4.3	2.3				0	6.6
BP	5, 15	2.9	2	dl400	4700	Cubic	0.01	11
GaP	31, 15	4.13	2.24	1750		Cubic		
CdS	48, 16	4.82	2.5	1477		Hexagonal	0.58	11.6
SiC	14, 6	3.2	2.2			Cubic		
AlSb	13, 51	4.26	1.62			Cubic		
PbO	82, 8	9.8	1.9	886				
BiI_3	83, 53	5.78	1.73	408		Hexagonal		
ZnSe	30, 34	5.42	2.58			Cubic		8.1

TABLE I (*Continued*)

E_{pair} eV	Resistivity (25°C) Ω-cm	Electron Mobility cm²/V · sec	Electron Lifetime sec.	Hole Mobility cm²/V · sec	Hole Lifetime sec.	$\mu\tau(e)$ Product cm²/V	$\mu\tau(h)$ Product cm²/V
2.96	50	3900	$>10^{-3}$	1900	1×10^{-3}	>1	>1
3.62	up to 10^4	1400	$>10^{-3}$	480	2×10^{-3}	>1	≈1
4.43	10^9	1100	3×10^{-6}	100	2×10^{-6}	3.3×10^{-3}	2×10^{-4}
5.0*	10^{11}	1350	10^{-6}	120	5×10^{-8}	1×10^{-3}	6×10^{-6}
5.5**	10^8	720	10^{-6}	75	10^{-6}	7.2×10^{-4}	7.5×10^{-5}
						$\approx 10^{-4}$	
4.2	10^{13}	100	10^{-6}	4	10^{-5}	10^{-4}	4×10^{-5}
	10^{10}					9×10^{-5}	
4.2	10^7	8000	10^{-8}	400	10^{-7}	8×10^{-5}	4×10^{-6}
	10^{11}					7×10^{-5}	
4.5		75	5×10^{-7}	45	2×10^{-7}	3.5×10^{-5}	9×10^{-5}
13.25		2000	10^{-8}	1600	$<10^{-8}$	2×10^{-5}	$<1.6 \times 10^{-5}$
6.5	10^{12}	6	2.5×10^{-6}			1.6×10^{-5}	1.5×10^{-6}
4.9	10^{12}	8	10^{-6}	2		8×10^{-6}	
4.2	10^7	4600	1.5×10^{-9}	150	$<10^{-7}$	4.8×10^{-6}	$<1.5 \times 10^{-5}$
7.0**	10^{10}	340	4×10^{-9}	100	7×10^{-7}	1.4×10^{-6}	7×10^{-5}
	5×10^{13}					1×10^{-6}	$<1 \times 10^{-7}$
4	10^{12}	1	6.8×10^{-9}	.005	4×10^{-6}	6.8×10^{-8}	2×10^{-8}
7	10^{12}	.005	10^{-6}	.14	10^{-6}	5×10^{-9}	1.4×10^{-7}
6.5**	1	10	10^{-9}				
7.0**		120		120			
7.8**		300		50			
9.0**		400(α)					
5.05	$<10^4$	300		400			
6.47							
5.5**	10^{12}						
8.0**		100					

Note: Materials are listed in order of decreasing $\mu\tau(e)$ at room temperature.
*Estimated for 20% Zn.
**Estimated.
†Solid/solid phase transition.

Semiconductors for Room Temperature Nuclear Detector Applications

SEMICONDUCTORS AND SEMIMETALS Volume 43

J. Ott et al, InP sensors for thin-film detectors

Device fabrication

- Single- and multipad devices fabricated by S. Kim at Argonne National Lab on commercial 2” InP:Fe wafers of 350 µm thickness
- Both sides 10 nm / 100 nm Cr / Au
  - Front side electrode design by e-beam evaporation and lift-off of patterned photoresist
  - Backside sheet metallization by sputter deposition

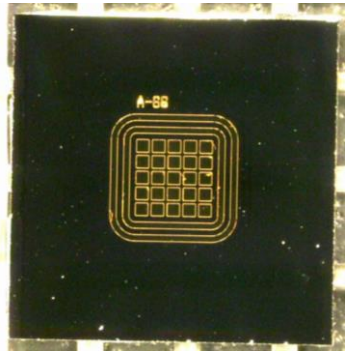

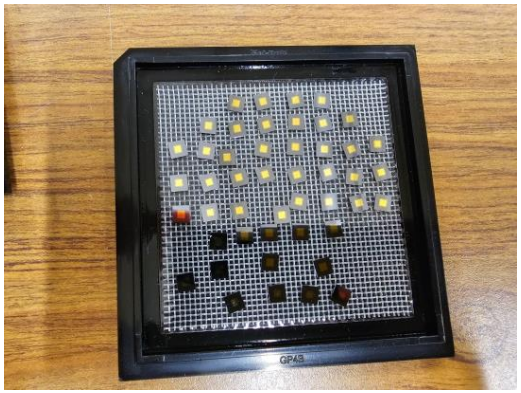

- Single pad devices: 2x2 mm, one guard ring (100 µm) – half of the devices with a 150 µm optical opening
- Multi-pad arrays: 25 pads, each 200x200 µm, 50 µm gap

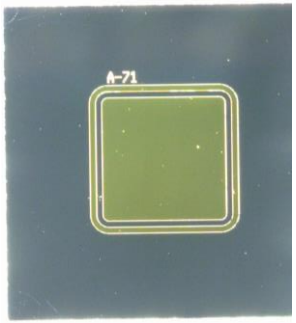

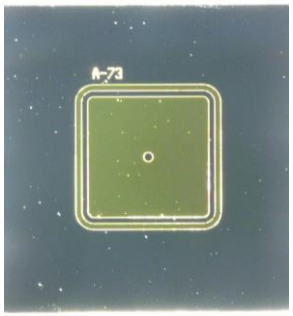

CV-IV characterization

- Capacitance for 2x2 mm pad: ca. 2 pF
- Leakage currents higher than in Si, on the µA/mm2 scale
  - Relatively symmetrical in polarity
  - Initially almost Ohmic behavior, then soft increase after 400 V
  - No exponential breakdown before 600 V
- Some samples exhibit rising capacitance and higher initial leakage current: apparently concentrated around a specific area on the wafer, close to a cut line

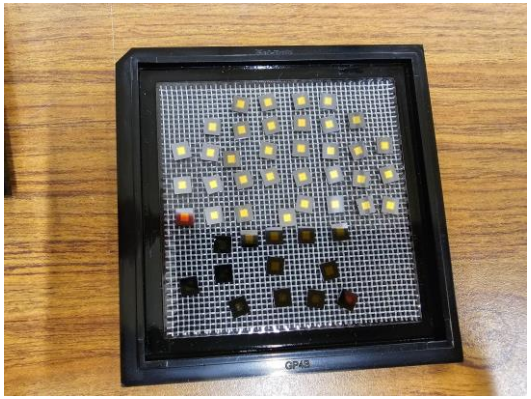

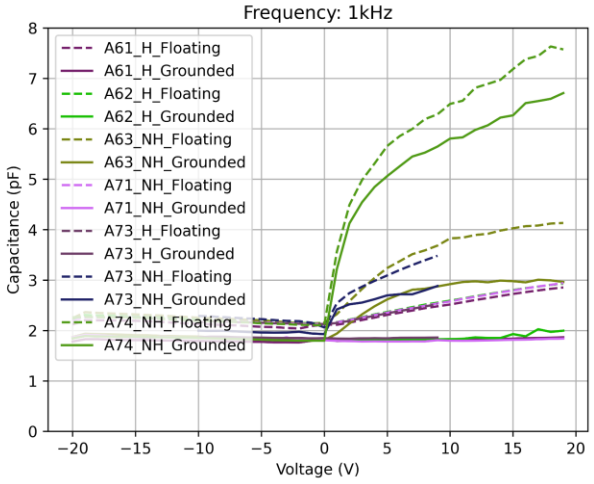

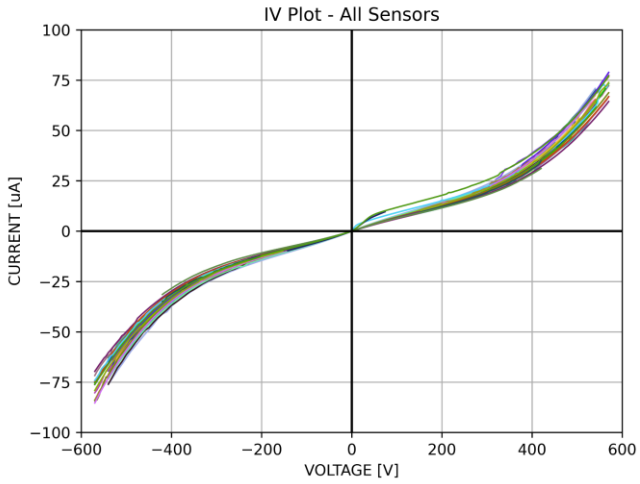

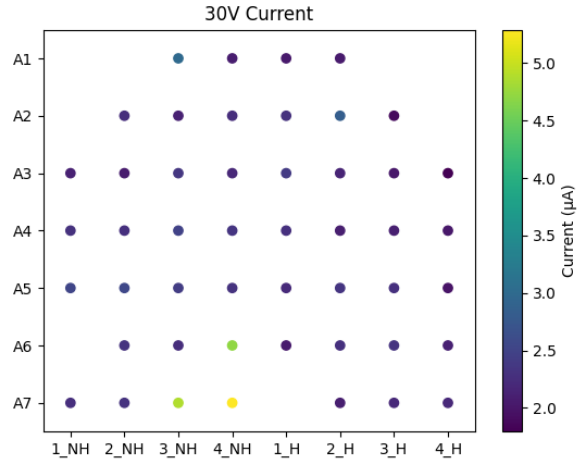

Single-pad devices

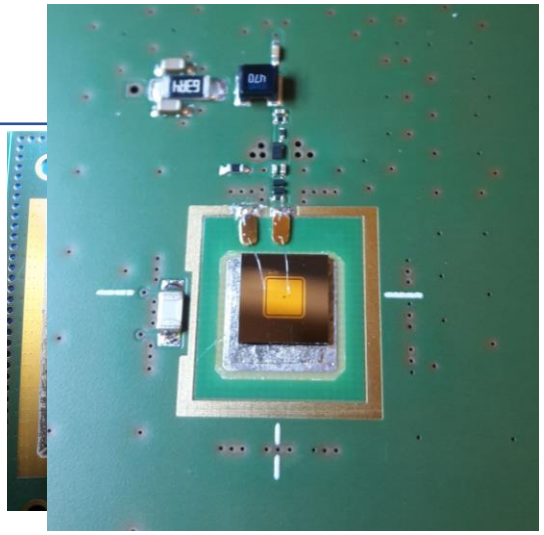

Sensor bonded to 1-ch UCSC fast readout board with 470 Ω transimpedance amplifier, plus external 20dB RF amplifier

- 638 nm red laser, x-y scanning stage (Particulars)
- Laser intensity adjusted manually to obtain 20 – 30 mV signal
- *No signal from the IR laser even at high intensities*

- Beta source: Sr-90
- Known HPK Silicon LGAD as trigger and reference

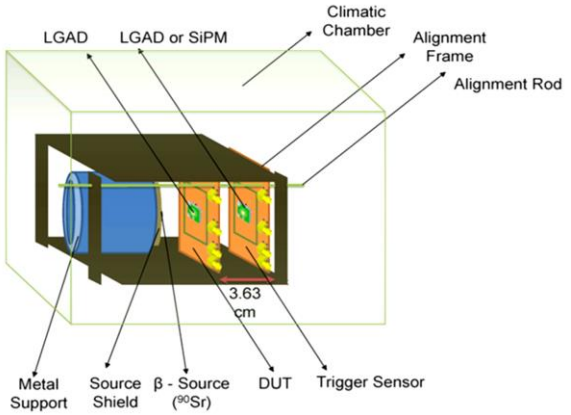

Z. Galloway et al 2019

Single-pad: laser

- Scanning over the central region of the device: contour of the optical opening well visible
- Strong gradient in signal maximum amplitude towards edge of the opening: not improved in refocusing
- Fast signals!

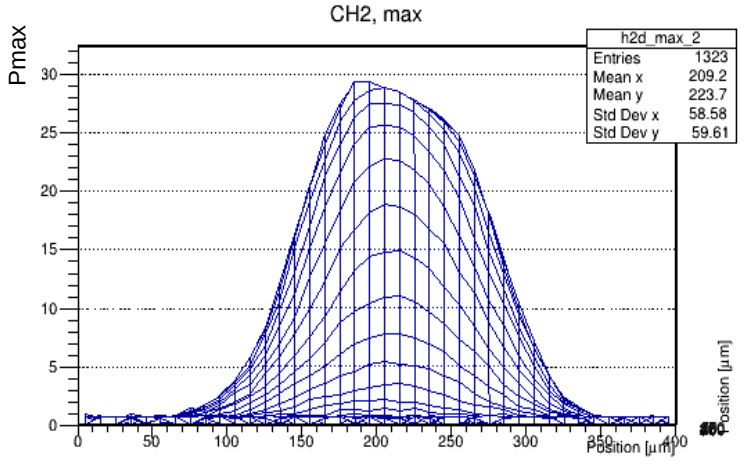

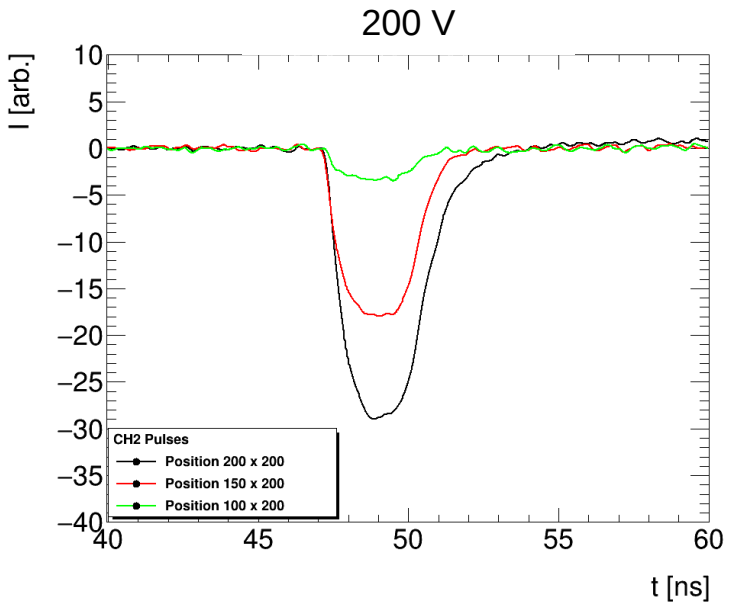

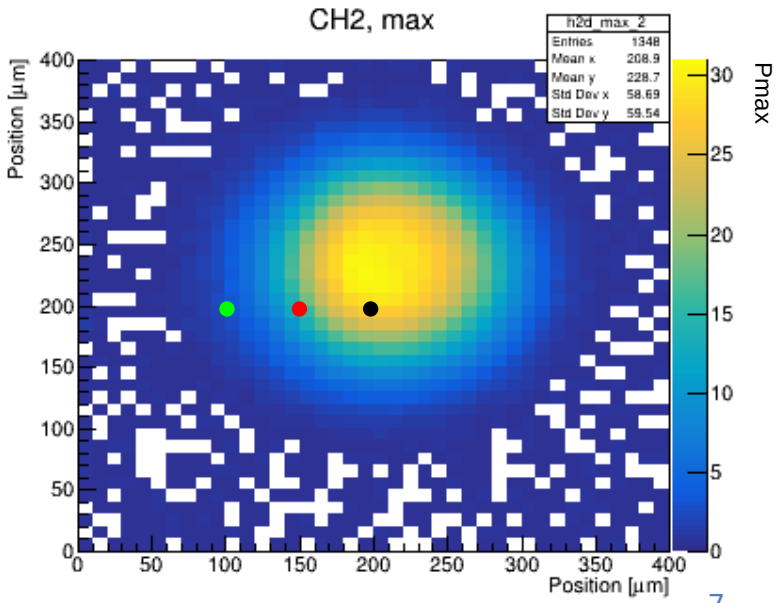

Single-pad: laser, bias voltage polarity

- Changed to a different HV voltage supply: bias with negative, or positive backside voltage i.e. signal primarily from drifting electrons
  - Early saturation of hole drift velocity?
  - Electrons: larger signals with long tail
    - ➢ Could be caused by charge multiplication / gain holes?
    - ➢Slow detrapping from defects in the bulk?

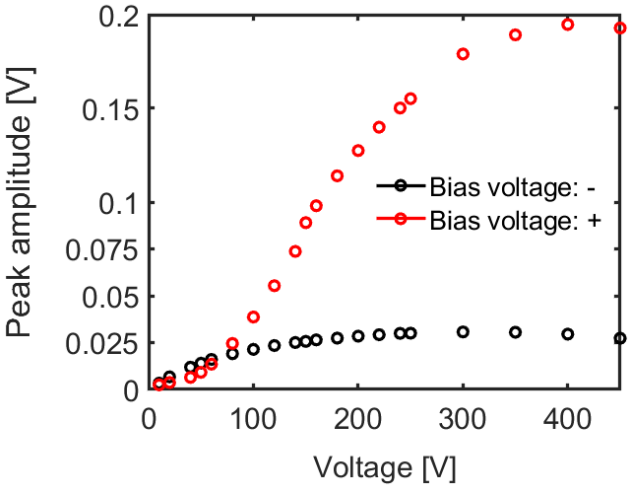

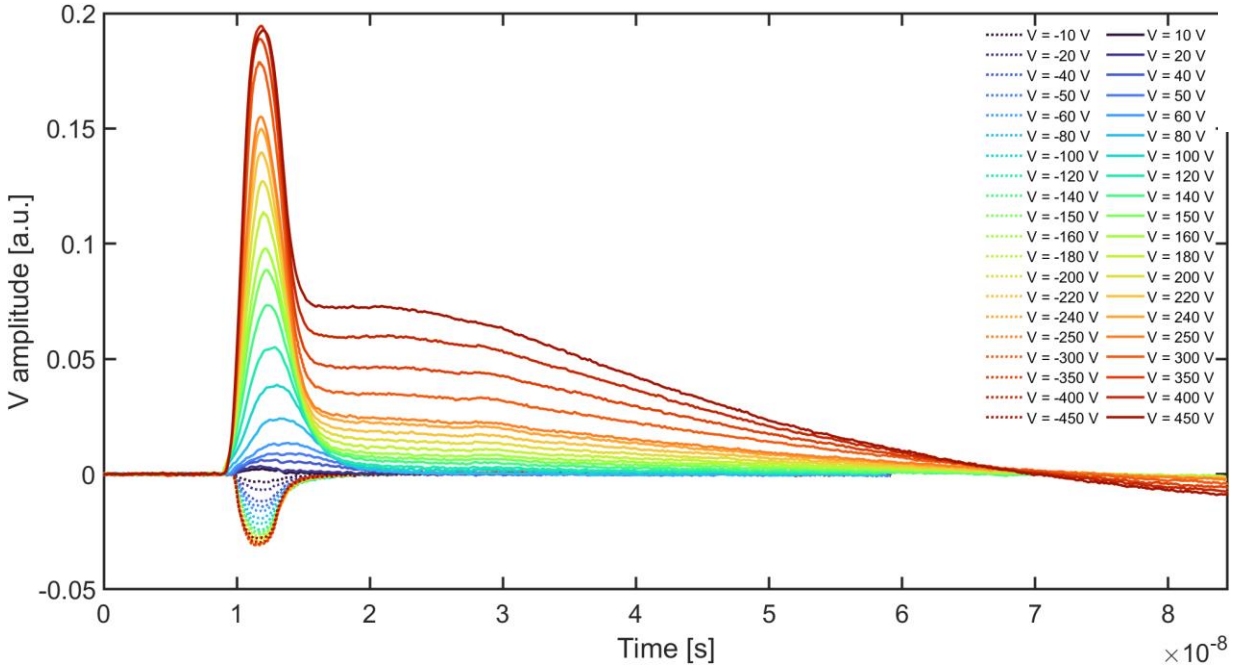

Sr-90 beta electrons: signals

- Practically independent of bias voltage polarity
  - ➢ Expected for homogeneous bulk and unsegmented single-pad electrode
- Comparatively small signal, around 15 mV, but fast
  - ➢ Similar, to laser signal from assumed hole drift, although a bit lower
- Decline after ca. 400 V
  - ➢ Similar to laser signal

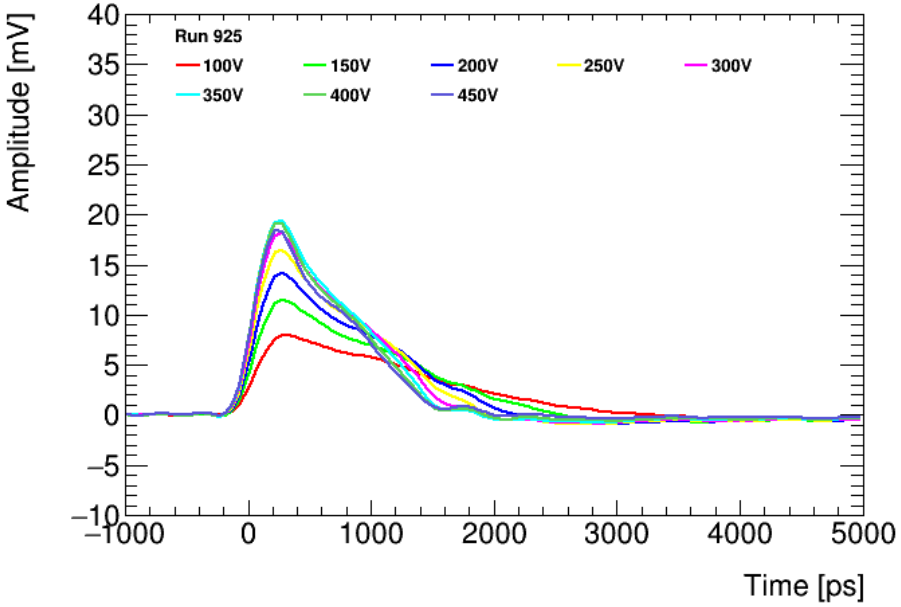

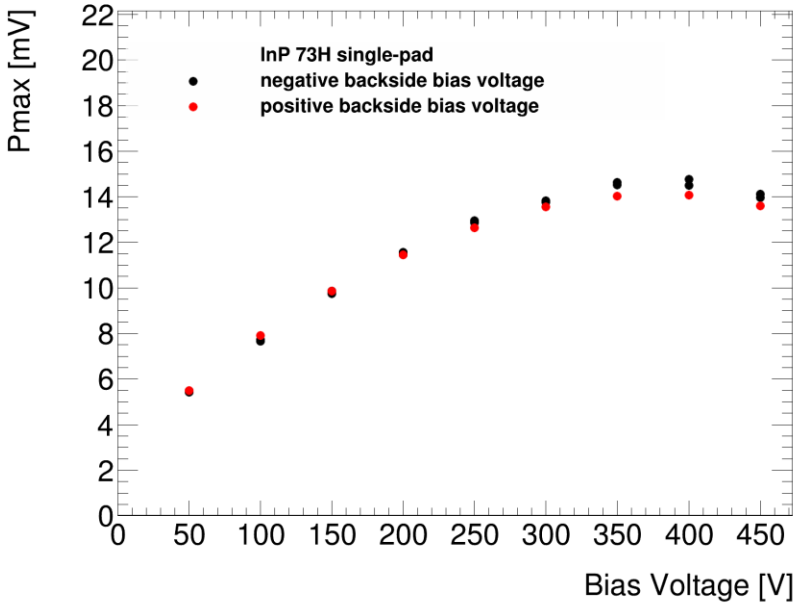

Sr-90 beta electrons: rise time and timing resolution

- Rise time independent of bias voltage, down to 250 ps after 150 V
- **Excellent timing resolution: 33 ps reached between 300 and 400 V**
  - Despite 350 µm-thick device, no special gain layer, relatively small signal!

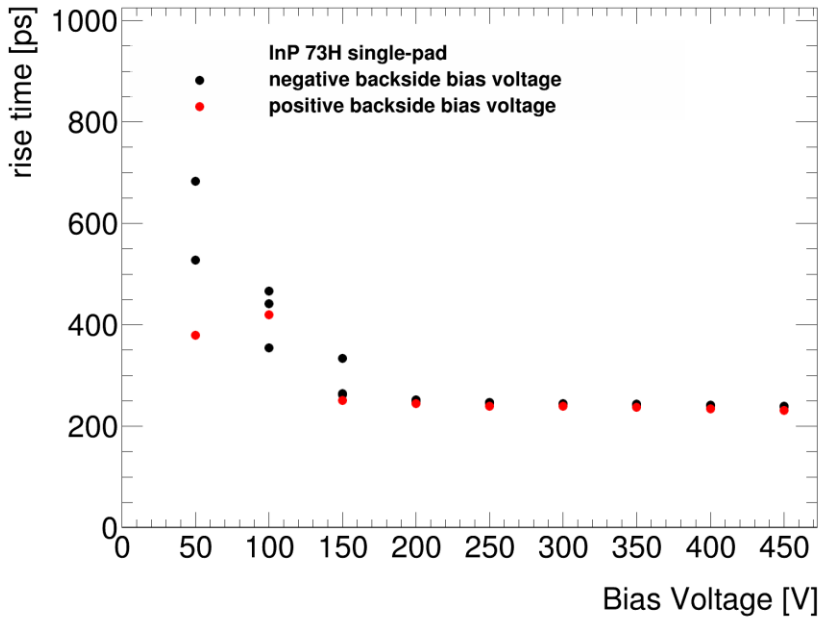

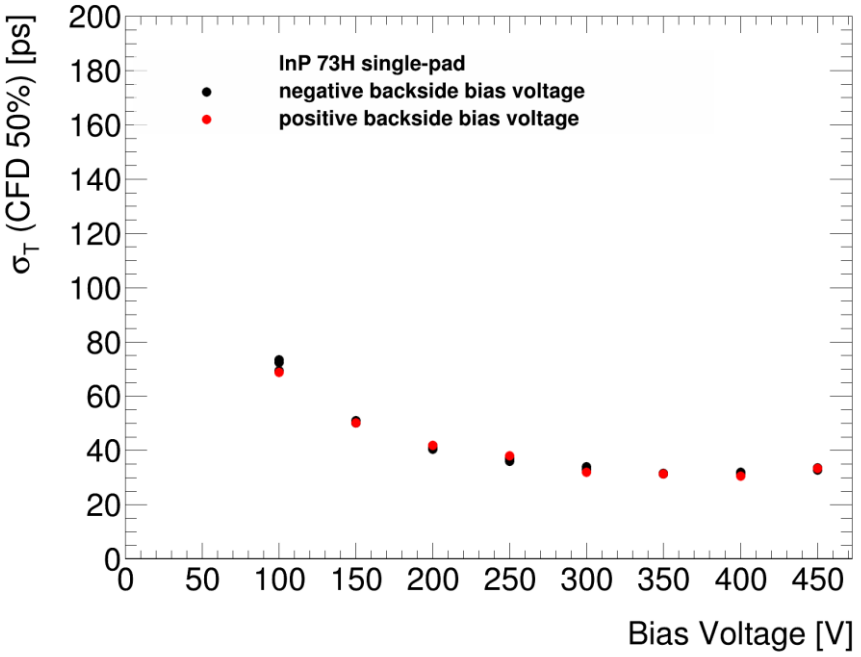

Multipad array: laser testing

- Same red laser, same intensity as for single pads
- + 250 V backside bias
- Sensor mounted on 16-ch Fermilab readout board
  - ➢ Remaining channels and guard ring originally planned to be grounded, but not feasible due to constrained space for wirebond loops – left floating
- Reading out 4 channels at a time

- Area A: adjacent pads
- Area B: larger area, finer granularity

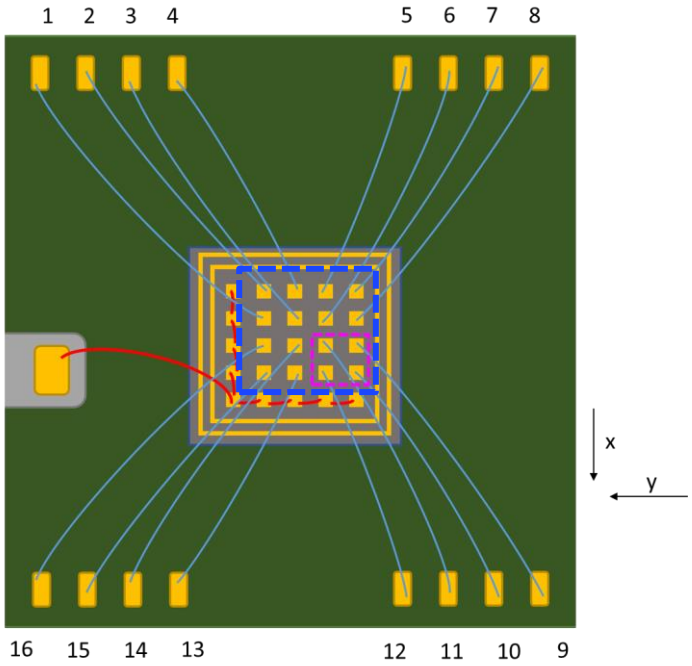

Area A: adjacent pads

- Large pulses close to pad
- Notable decrease in signal amplitude when charge is injected between pads – areas of lower efficiency even with only 50 µm inter-pad distance
- Inverted signal when charge is injected at neighboring pad (also seen relatively far away)

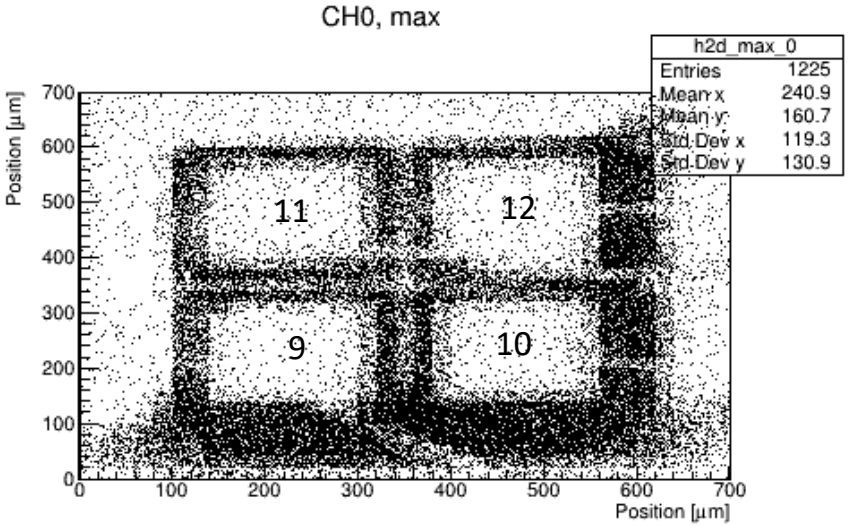

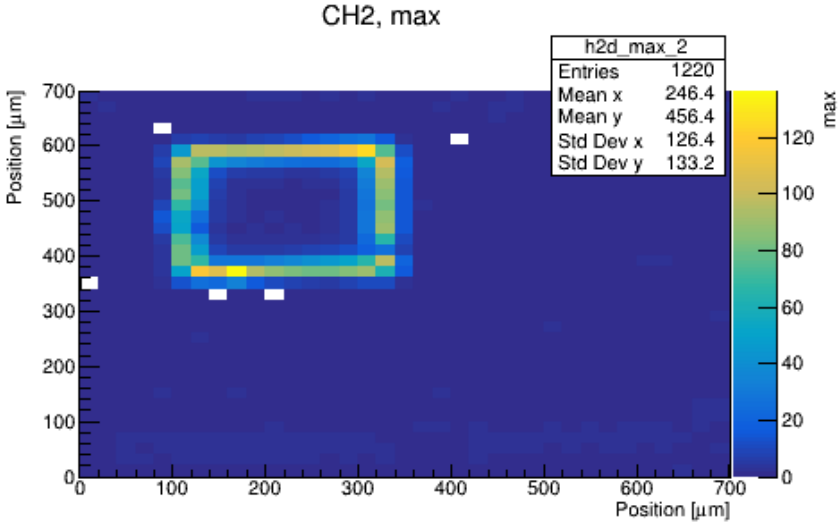

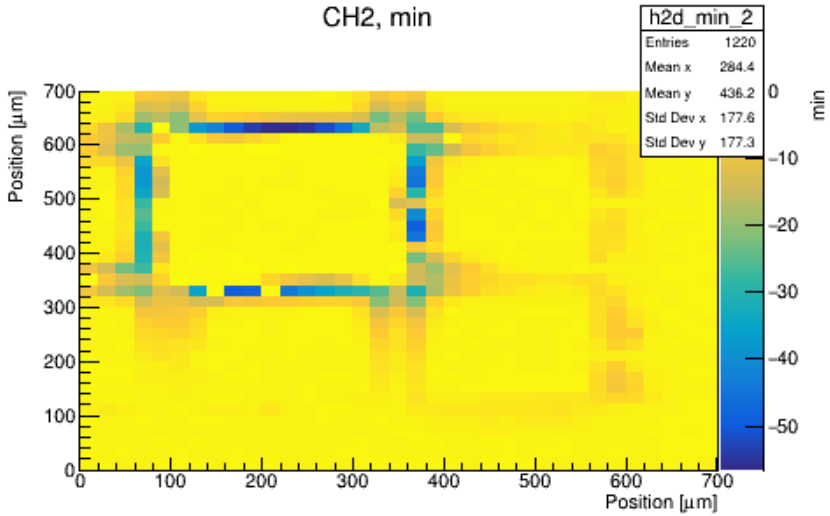

Area A: adjacent pads

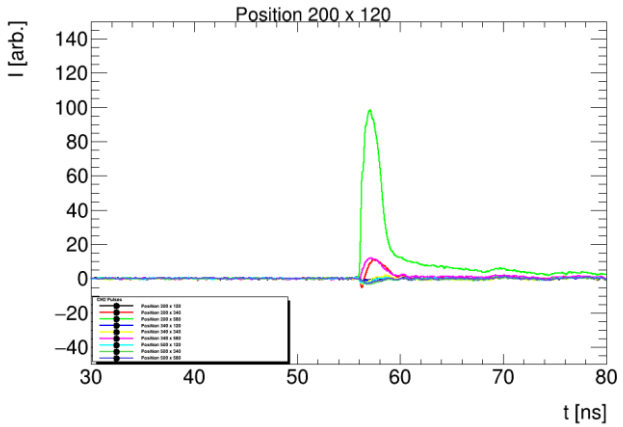

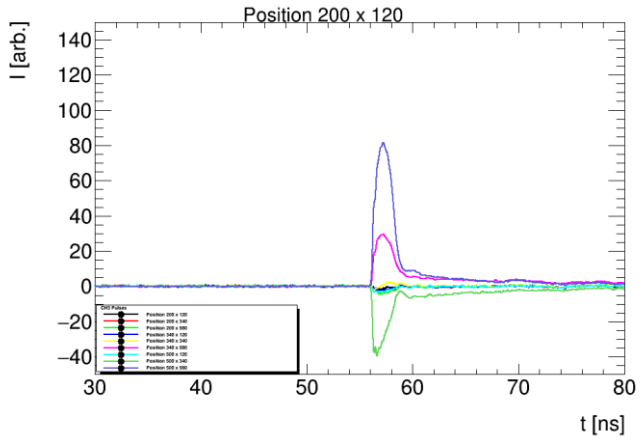

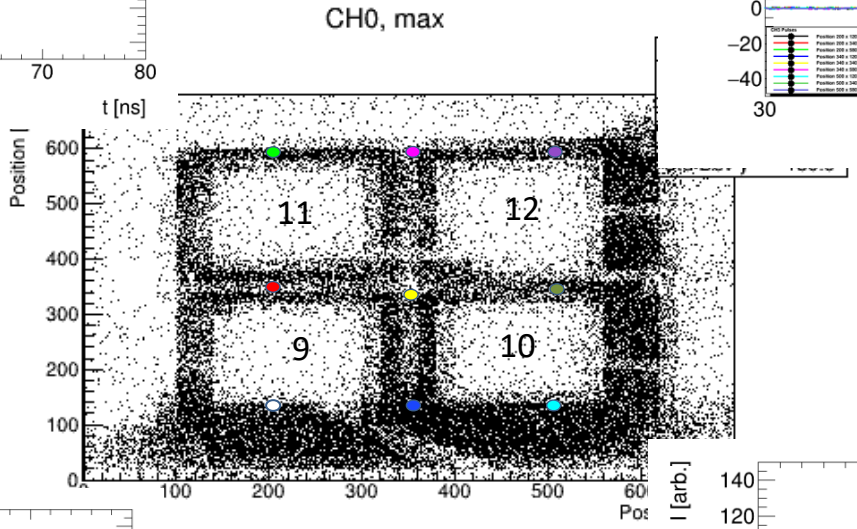

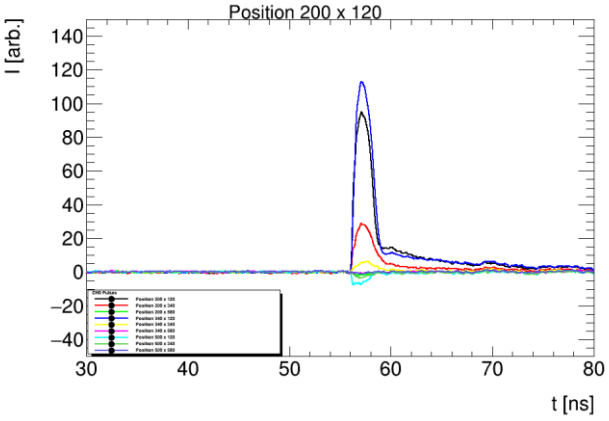

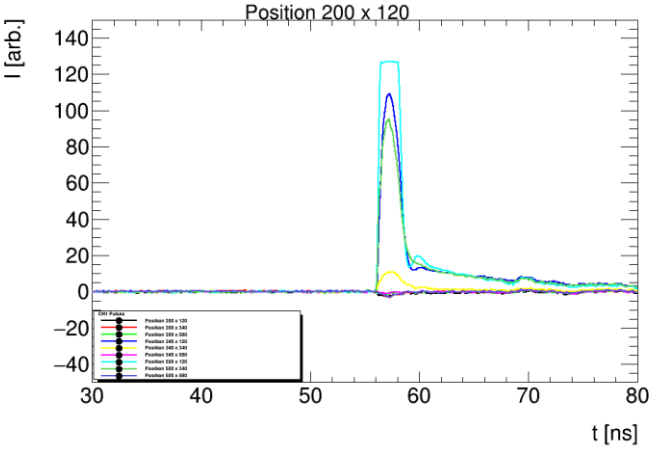

Area B: larger area, finer granularity

- Main signal is not shared far away: limited to < 50 µm
- Opposite-polarity signal observed along the neighboring pads - detectable for longer distance

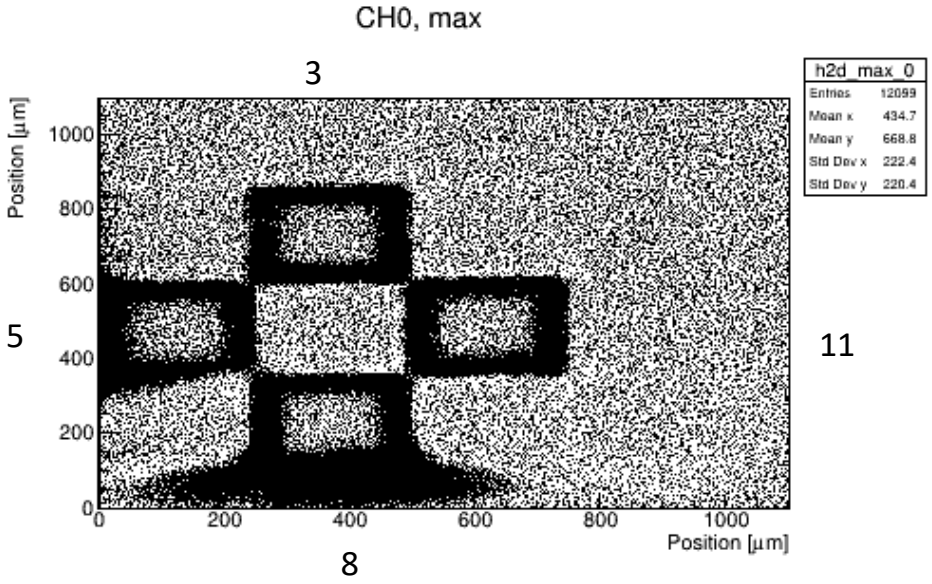

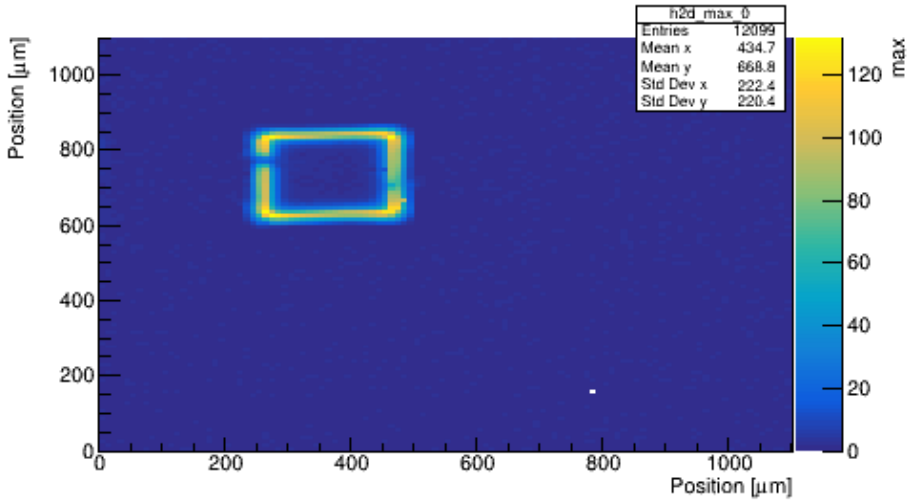

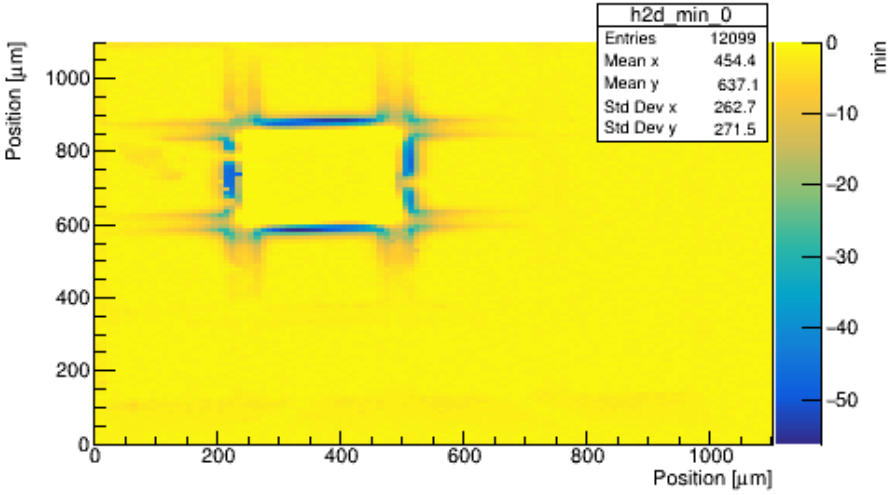

J. Ott et al, InP sensors for thin-film detectors

Area B: larger area, finer granularity

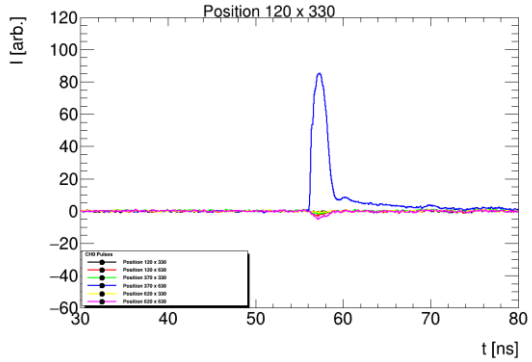

3

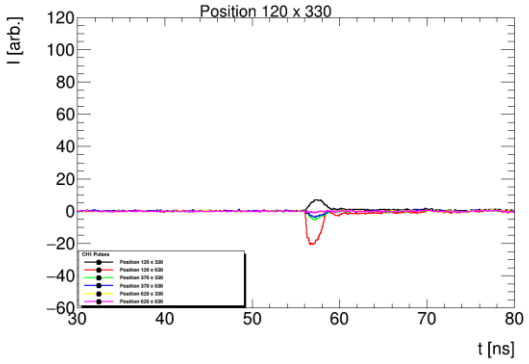

5

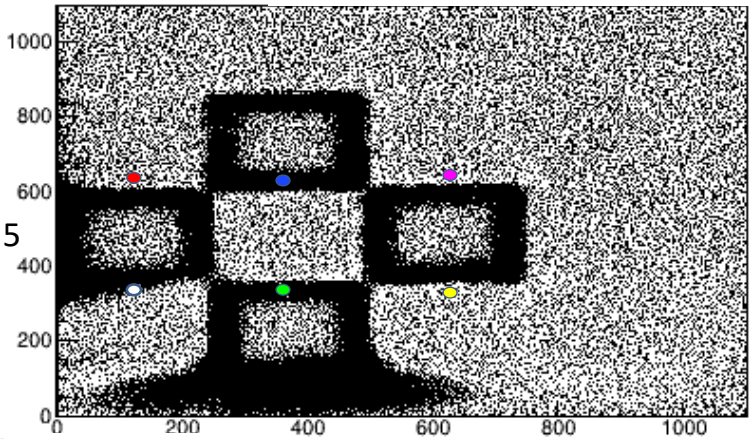

11

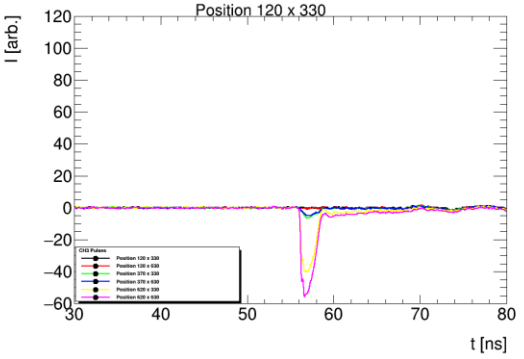

8

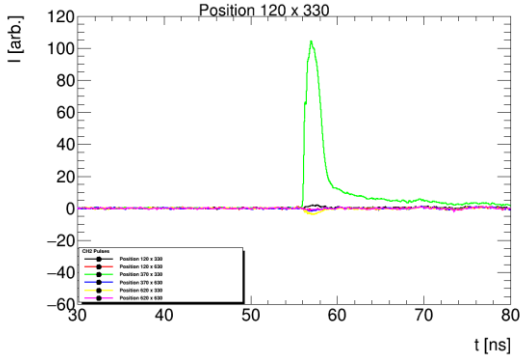

Amplitude profiles

- Main and opposite-polarity signals along one line across pads:
  - Opposite-polarity signal can reach up to 40-50 % of main signal amplitude
  - Mirrors the profile of the next pad's pulse maximum
  - Gap between pads recognizable

Area A

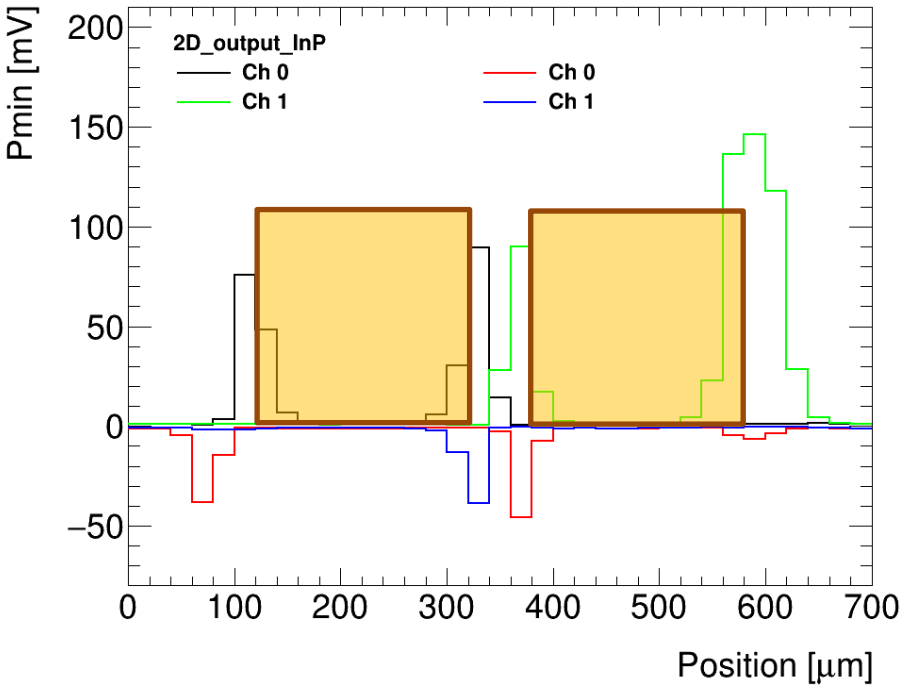

Area B

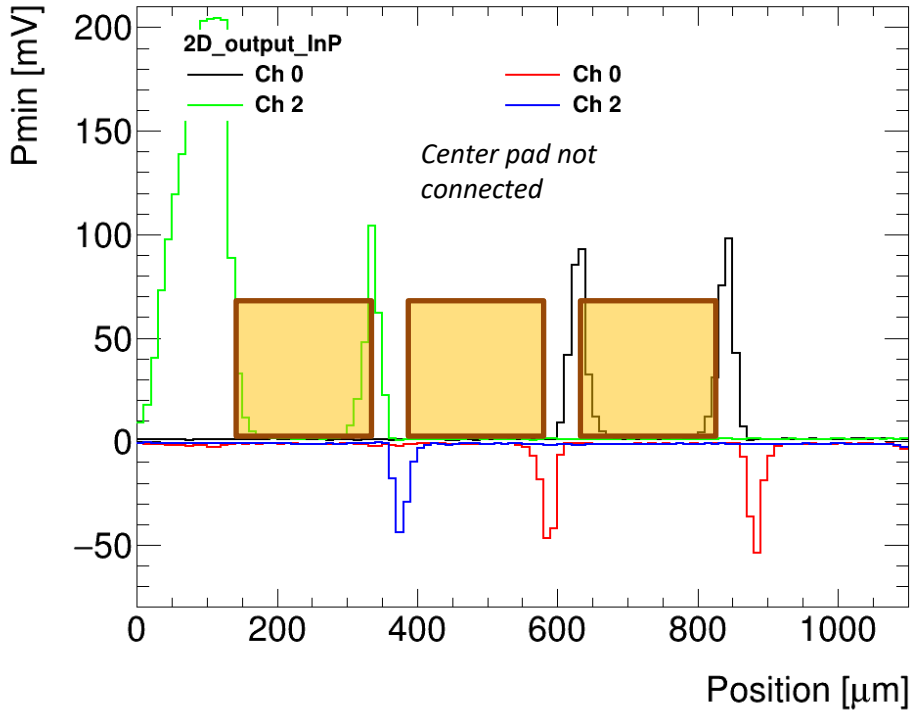

J. Ott et al, InP sensors for thin-film detectors

Polarity!

- In fact, large signals are also observed at negative backside bias! This is very different from the behavior of the single-pad sensor
  - ➢ Weighting field? Enhanced lateral drift of charges between pads?
- Better charge collection but worse resolution of features for negative bias

+250 V

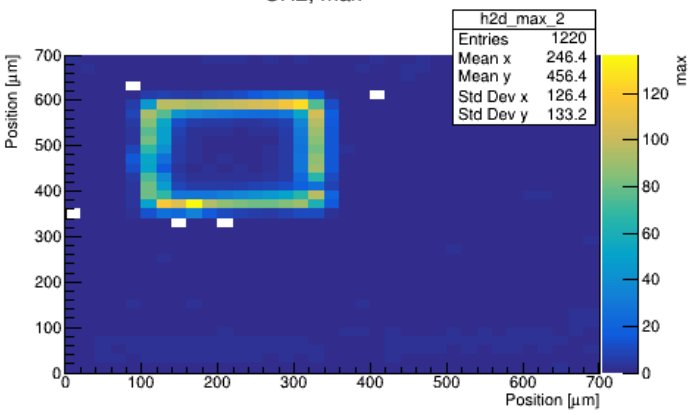

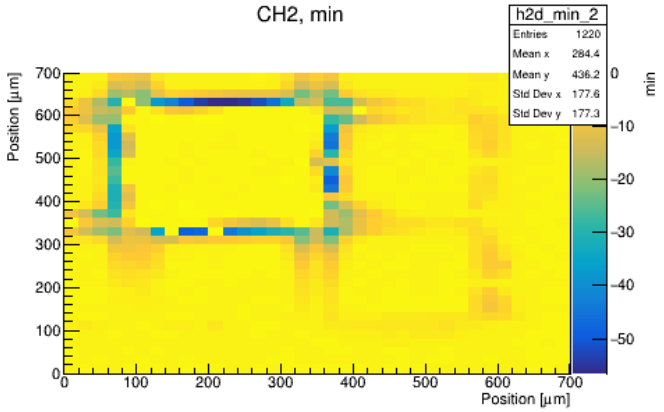

-250 V

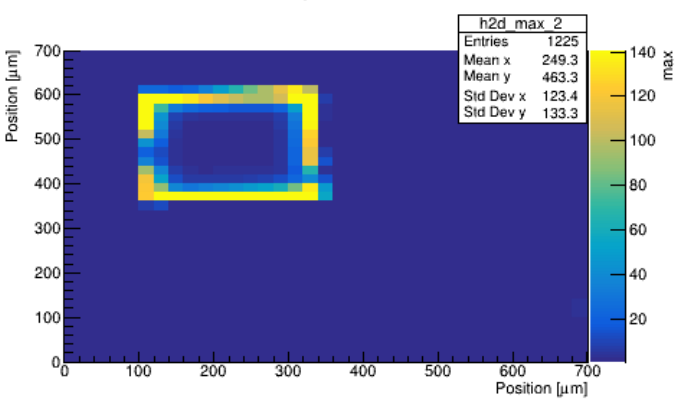

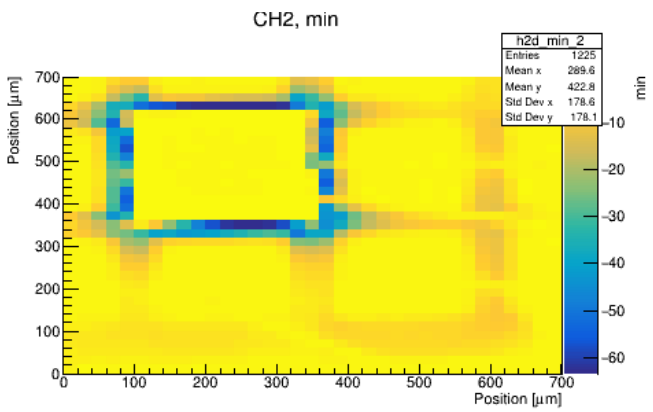

X-ray test beams

courtesy L. Poley and other collaborators

- X-ray test beams were conducted at CLS, Canada and Diamond, UK

- Shown here: two InP single-pad samples in CLS beam, 15 keV, diameter ca. 40 µm
  - ➢ Low bias voltage data has been analysed to study the response, response uniformity, and bias dependence
  - ➢ Loss of features in scans with increasing voltage, and 'flares' at the edge of the sensors under investigation

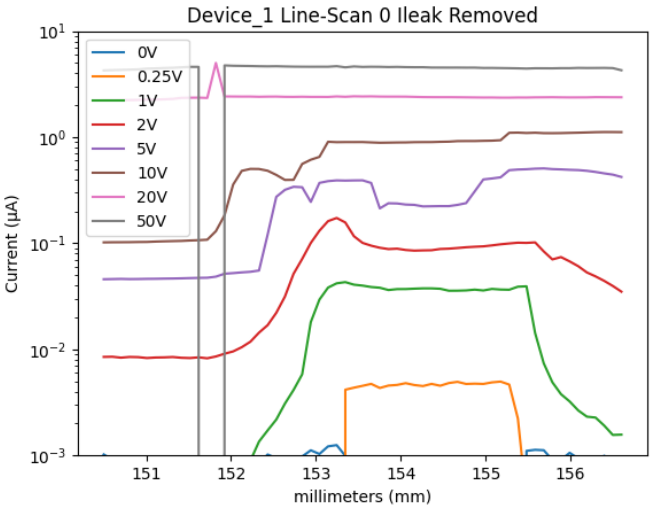

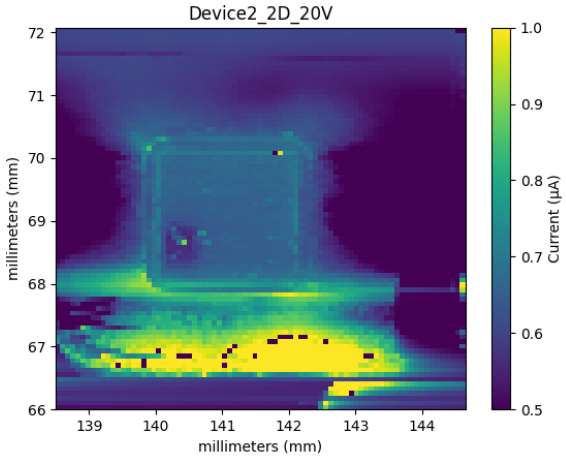

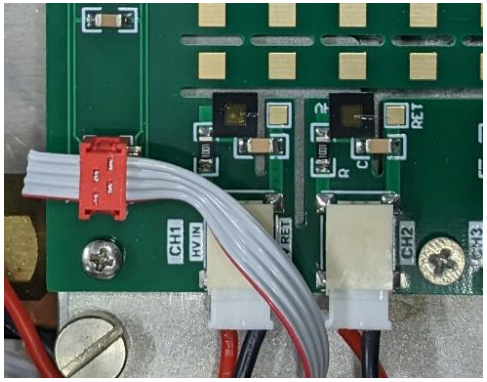

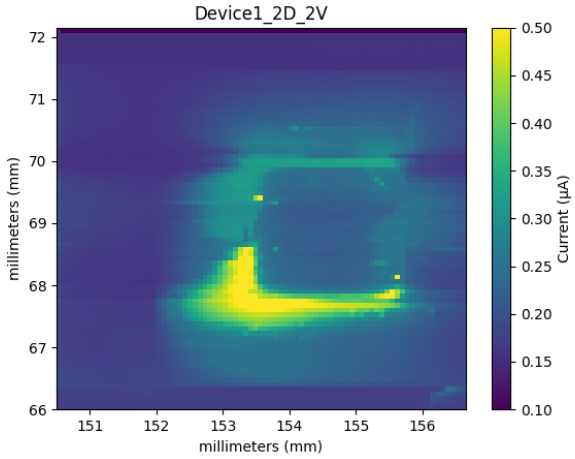

Summary and outlook

- Indium phosphide is a promising thin-film detector material: single pad and multipad arrays were fabricated on bulk material and studied with several methods
- In particular, high electron mobility leads to very fast signals and great timing resolution even at lower amplitude and in a thick detector
- Going towards a thinner bulk (or an actual thin film) could reduce both drift time and trapping, and start internal charge multiplication at lower absolute bias voltage - on the other hand, if there is no gain mechanism, an acceptable signal level might not be reached with a thinner sensor

- **Next steps:**
  - Testing of devices at Fermilab 120-GeV proton beam
  - SCIPP Alibava setup was in repair, will be set up when received back
  - Simulations with Allpix2, TCAD
  - Evaluate radiation hardness: samples to be sent to JSI/Ljubljana for neutron irradiation; potential irradiation campaigns with protons and gamma rays depending on availability
  - Thin film deposition with Argonne CVD setup..? Other materials, e.g. amorphous Se, available at SCIPP?

SCIPP
SANTA CRUZ INSTITUTE FOR PARTICLE PHYSICS
UC SANTA CRUZ

CHEMICAL ENGINEERING
COLLEGE OF ENGINEERING
UIC

Argonne
NATIONAL LABORATORY

SUOMEN KULTTUURIRAHASTO

Thank you!

Charge collection

- C.C. based on beta electrons